International Journal of Biochemistry and Cell Biology 116 (2019) 105622

Contents lists available at ScienceDirect

International Journal of Biochemistry and Cell Biology

journal homepage: www.elsevier.com/locate/biocel

Inflammatory role of extracellular sphingolipids in Cystic Fibrosis

Aida Zulueta[a], Valeria Peli[a], Michele Dei Cas[a], Michela Colombo[b,g], Rita Paroni[a], Monica Falleni[c], Alessandro Baisi[d], Valentina Bollati[e], Raffaella Chiaramonte[b], Elena Del Favero[f], Riccardo Ghidoni[a], Anna Caretti[a,*]

[a] Biochemistry and Molecular Biology Lab., Health Sciences Department, University of Milan, Via A. di Rudinì, 8, Milan, Italy
[b] Laboratory of Experimental Medicine and Pathophysiology, Health Sciences Department, University of Milan, Via A. di Rudinì, 8, Milan, Italy
[c] Pathology Division, Health Sciences Department, University of Milan, San Paolo Hospital Medical School, Via A. di Rudinì, 8, Milan, Italy
[d] Thoracic Surgery Unit, Health Sciences Department, University of Milan, San Paolo Hospital Medical School, Via A. di Rudinì, 8, Milan, Italy
[e] EPIGET LAB, Department of Clinical Sciences and Community Health, University of Milan, Milan, Italy
[f] Department of Medical Biotechnology and Translational Medicine, University of Milan, Via Fratelli Cervi 93, Milan, Italy
[g] Haematopoietic Stem Cell Biology Laboratory, Medical Research Council(MRC) Weatherall Institute of Molecular Medicine (WIMM), University of Oxford, Oxford OX39DS, UK

ARTICLE INFO

Keywords:
Sphingolipids
Ceramide
Inflammation
Extracellular vesicles
Mesenchymal stem cells

ABSTRACT

Ceramide is emerging as one of the players of inflammation in lung diseases. However, data on its inflammatory role in Cystic Fibrosis (CF) as part of the extracellular machinery driven by lung mesenchymal stem cells (MSCs)-derived extracellular vesicles (EVs) are missing.

We obtained an *in vitro* model of CF-MSC by treating control human lung MSCs with a specific CFTR inhibitor. We characterized EVs populations derived from MSCs (ctr EVs) and CF-MSCs (CF-EVs) and analyzed their sphingolipid profile by LC–MS/MS. To evaluate their immunomodulatory function, we treated an *in vitro* human model of CF, with both EVs populations.

Our data show that the two EVs populations differ for the average size, amount, and rate of uptake. CF-EVs display higher ceramide and dihydroceramide accumulation as compared to control EVs, suggesting the involvement of the *de novo* biosynthesis pathway in the parental CF-MSCs. Higher sphingomyelinase activity in CF-MSCs, driven by inflammation-induced ceramide accumulation, sustains the exocytosis of vesicles that export new formed pro-inflammatory ceramide.

Our results suggest that CFTR dysfunction associates with an enhanced sphingolipid metabolism leading to the release of EVs that export the excess of pro-inflammatory Cer to the recipient cells, thus contributing to maintain the unresolved inflammatory status of CF.

1. Introduction

Long considered structural and metabolic molecules, sphingolipids (SPLs) have been recognized as signaling mediators. SPLs are localized in the plasma and in intracellular organelle membranes, with ceramide (Cer) being the structural unit of membrane-forming SPLs and the main modulator of cellular processes such as cell growth, cell death and inflammation (Hannun and Obeid, 2008; Chiricozzi et al., 2018). Cer can derive from the *de novo* biosynthesis pathway or from the so-called salvage pathway via degradation of complex SPLs, such as sphingomyelin (SM), the most abundant membrane lipid (Gault et al., 2010; Marchesini and Hannun, 2004). Among sphingolipids, Cer is emerging as one of the players of the pulmonary dysfunction in inflammatory lung diseases, such as Chronic Obstructive Pulmonary Disease (COPD) and Cystic Fibrosis (CF) (Petrache and Petrusca, 2013; Grassme et al., 2013). Its accumulation in the airways of CFTR-deficient mice, is related to pulmonary inflammation, death of epithelial cells, and susceptibility to severe *P. aeruginosa* infections in mice and in human (Teichgraber et al., 2008; Riethmuller et al., 2009; Becker et al., 2010). We previously demonstrated that the *de novo* ceramide synthesis contributes to lung inflammation and *P. aeruginosa* infection in a murine CF model (Caretti et al., 2014). Moreover, we observed that reducing

* Corresponding author.
E-mail addresses: aida.zulueta@unimi.it (A. Zulueta), valeria.peli@unimi.it (V. Peli), michele.deicas@unimi.it (M. Dei Cas), michela.colombo1@unimi.it (M. Colombo), rita.paroni@unimi.it (R. Paroni), monica.falleni@unimi.it (M. Falleni), alessandro.baisi@unimi.it (A. Baisi), valentina.bollati@unimi.it (V. Bollati), raffaella.chiaramonte@unimi.it (R. Chiaramonte), elena.delfavero@unimi.it (E. Del Favero), riccardo.ghidoni@unimi.it (R. Ghidoni), anna.caretti@unimi.it (A. Caretti).

https://doi.org/10.1016/j.biocel.2019.105622
Received 3 May 2019; Received in revised form 24 September 2019; Accepted 25 September 2019
Available online 26 September 2019

ceramide accumulation in CF airways, correlates with an up-regulation of the anti-oxidative response of the transcriptional factor NRF2, even under infection by *A. fumigatus* (Caretti et al., 2016) and with a down-regulation of the pro-inflammatory cytokine release (Caretti et al., 2014).

Mesenchymal stem cells (MSCs) are multipotent non-hematopoietic stem cells residing in many tissues, including the lung, with an emergent role in the attenuation of inflammation mainly due to the release of extracellular vesicles (EVs). EVs are membrane-derived particles that comprise both exosomes and microvesicles (MVs). Exosomes are generated inside multivesicular bodies (MVB) and are generally 30–100 nm in diameter. Microvesicles are derived from the plasma membrane and are generally larger than exosomes, ranging from 100 to 300 nm. They are involved in intercellular communication since they carry a large array of bioactive molecules including proteins, mRNA, miRNA and bioactive lipids to distant cells (Fatima et al., 2017; Dostert et al., 2017). We have recently demonstrated the role of EVs produced by human lung MSCs in controlling inflammation process. In an *in vitro* CF bronchial epithelial cellular model, EVs treatment reduces transcription and protein expression of pro-inflammatory cytokines such as IL-1β, IL-8, IL-6, under basal and TNFα stimulated conditions. This effect could be mediated by up-regulation of the PPARγ axis, whose down-stream effectors (NF-kB and HO-1) are well-known modulators of inflammatory and oxidative stress pathways (Zulueta et al., 2018).

SPLs participate in EVs biogenesis and in EVs activity towards target cells, as reviewed by Verderio C. and colleagues (Verderio et al., 2018). Cer derived from SM hydrolysis, promoted by neutral sphingomyelinase 2 (n-SMase2), drives exosomes formation and transport via an ESCRT-independent pathway (Trajkovic et al., 2008). Secretion of neuron-derived exosomes was modulated by the activities of sphingolipid-metabolizing enzymes, including nSMase2, in Alzheimer disease models (Yuyama et al., 2012; Dinkins et al., 2014). As for MVs, the acid sphingomyelinase generates Cer that in turn triggers MVs budding from the plasma membrane (Bianco et al., 2009). SM to Cer conversion alters membrane curvature and fluidity, driving membrane evagination of MVs by means of redistribution of inverted cone-shaped Cer molecules (Subra et al., 2007). Several lines of evidence indicate Cer-enriched exosomes as mediators of cytotoxic effects in target cells. Primary cultured astrocytes secrete prostate apoptosis response 4 (PAR-4)/ceramide-enriched exosomes that represent a novel mechanism of Aβ-dependent apoptosis in Alzheimer disease (Wang et al., 2012). More recently, Podbielska M. and colleagues, demonstrated the pro-apoptotic potential of Cer-enriched exosomes released by a human oligodendroglioma cell line previously stimulated with inflammatory cytokines (Podbielska et al., 2016).

In the present manuscript, we investigated the hypothesis that lung MSCs and MSCs-derived EVs could be immunologically impaired in CF, partially because of altered SPLs content. By means of an *in vitro* model of CF-MSCs, we found higher ceramide and dihydroceramide (dhCer) content in EVs shed from CF-MSCs (CF-EVs) than in control MSCs-derived EVs (ctr EVs), with C16:0 and the long acyl chain ceramides (C22:0; C24:0; C24:1) being the most representative. Moreover, the two EV populations are different in term of average size, amount, and rate of uptake by the recipient cells. As for parental MSCs, total Cer and sphingomyelin content significantly increased and decreased, respectively. By treating IB3-1, a bronchial epithelial cell line derived from a CF patient, with CF-EVs or ctr EVs, we observed that CF-EVs are less efficient in decreasing pro-inflammatory cytokines expression. Overall, we observed an inverse correlation between the anti-inflammatory efficacy of EVs and their Cer content.

In conclusion, our data suggest that lung MSCs compartment may be immunologically altered in CF thus contributing to maintain the chronic, unresolved pulmonary inflammation.

2. Materials and methods

2.1. Reagents and antibodies

The following materials were purchased: bFGF and TNFα from Peprotech LTD (Israel); LHC Basal, LHC-8 w/o gentamicin culture media from Gibco (US); FBS and DMEM from Euro Clone Life Science Division (Italy); protease inhibitors (Roche Italia, Italy); CellBrite Green Cytoplasmic Membrane Dye (Biotium, US); SYBR Green system (Qiagen, Italy); synthetic oligonucleotides from M-Medical (Italy), I-172 CFTR inhibitor (Sigma Aldrich, DE). Methanol, acetonitrile, ammonium formate, acetic acid, potassium hydroxide and formic acid (all analytical grade) were supplied from Merck (Darmstadt, Germany). Water was MilliQ grade. Sphingolipids standards were purchased by Avanti Polar Lipids (Alabaster, USA). Primary antibodies: anti- PPARγ (ElabScience, US), anti-H3 (Cell Signaling, US), anti-β-actin (Sigma, US), anti-CFTR Type A4 (596) (University of North Carolina – Chapel Hill, UNC-CH, on behalf of Cystic Fibrosis Foundation, USA), anti-HO-1 (Abcam, UK), anti-caspase 9 (Cell Signaling, US), anti-LC3 (Cell Signaling, US). The secondary antibodies were from Jackson Laboratories (Bar Harbor, ME, US). All reagents were of the maximal available purity degree.

2.2. Ethic statements

Human lung mesenchymal stem cells (MSCs) were isolated from lung biopsies obtained from seven patients that underwent lung surgery for suspected bullous emphysema or lung tumor. Tissues were obtained under appropriate approval by the Ethical Committee of the ASST Santi Paolo e Carlo, Milano, Area A (n°2211, 12/14/2016). All participants signed informed consent forms approved by the Ethical Committee before surgery and specimen collection. All the procedures followed the Declaration of Helsinki protocols.

2.3. Isolation and treatment of human lung MSCs

Human lung MSCs were isolated and cultured as previously described (Zulueta et al., 2018). Briefly, lung samples were recovered after planned surgery for non infectious diseases (bullous and tumor lesions). Each lung biopsy of about 1 cm^3, was minced with surgical scissors and maintained in DMEM medium containing 18% FBS and 1% penicillin/streptomycin at 37 °C in a humid atmosphere containing 5% CO_2 for ten days. At day tenth, the adherent cells were cultured continuously in the presence of bFGF (5 ng/mL) until the passage seven. To obtain an *in vitro* model of Cystic Fibrosis MSCs (CF-MSCs), control MSCs (ctr MSCs) were treated with 10 μg/ml of I-172 CFTR inhibitor for 48 h, as reported by Mattoscio et al (Mattoscio et al., 2010). Control MSCs are intended as treated with dimethyl sulfoxide (DMSO), the I-172 CFTR inhibitor's solvent.

2.4. Isolation of Extracellular vesicles (EVs) derived from human lung MSCs

EVs were obtained from the supernatants of both ctr- and CF-MSCs cultures (ctr EVs and CF-EVs, respectively) after 48–72 hours, by ultracentrifugation as previously described (Bonzini et al., 2017). After serial centrifugations (1000, 2000 and 3000 *g* for 15 min at 4 °C), supernatants were centrifuged at 110,000 *g* (Beckman Coulter Optima L-90 K ultracentrifuge) for 75 min at 4 °C. EVs were resuspended according to the final MSCs number (10 μl per 1 × 10^6 cells).

2.5. Cell line and treatments

IB3-1 cells, an adeno-associated virus-transformed human bronchial epithelial cell line derived from a CF patient (ΔF508/W1282X) provided by LGC Promochem (US), were grown in LHC-8 medium

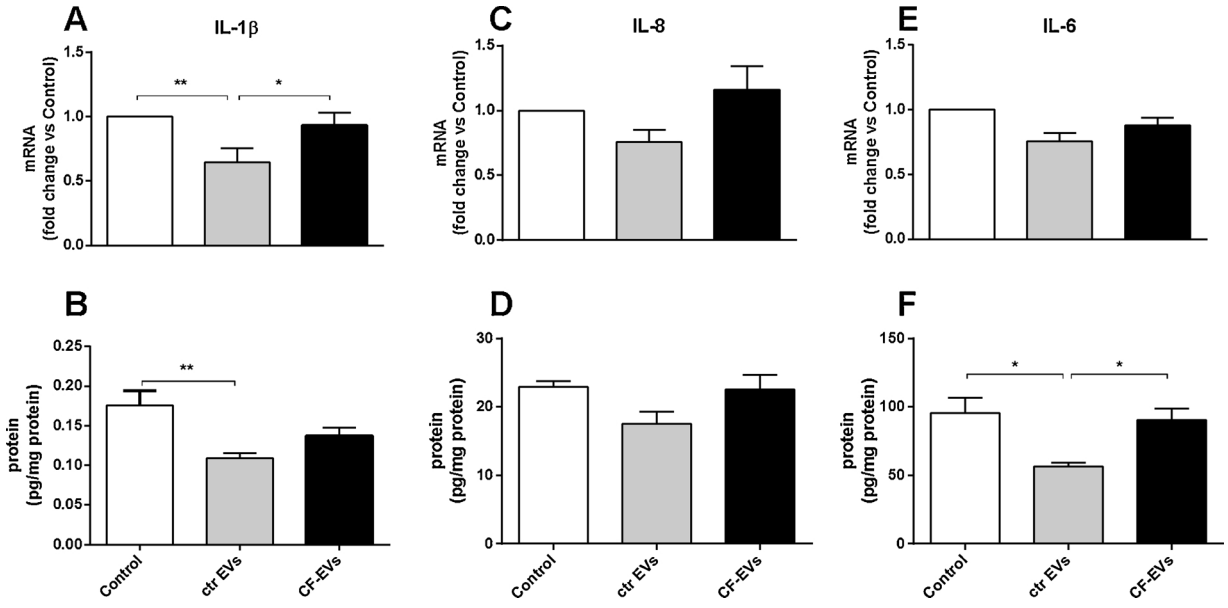

Fig. 1. Effects of EVs derived from ctr and CF-MSCs on cytokines mRNA expression and protein release in IB3-1 cells. The mRNA expression was evaluated by RT-PCR and the results reported as fold change over the control untreated IB3-1 cells. The cytokines content, expressed as picograms per mg of protein (pg/mg), was measured by ELISA in culture media of IB3-1 cells. Panel **A** and **B** refer to IL-1β mRNA and protein; panel **C** and **D**, to IL-8 mRNA and protein; panel **E** and **F**, to IL-6 mRNA and protein, respectively. Control refers to untreated IB3-1 cells at basal condition; ctr EVs refers to cells treated for 24 h with EVs from control MSCs; CF-EVs refers to cells treated for 24 h with EVs from CF-MSCs, meaning MSCs supplemented with 10 μg/ml of CFTR inhibitor, I-172, for 48 h. Data, expressed as mean ± SEM, are obtained from seven individual MSCs - derived EVs populations. The samples were run in triplicate for RT-PCR or in duplicate for ELISA analysis. Significance was evaluated by one-way ANOVA, followed by Newman-Keuls post-test. **, $p < 0.01$; *, $p < 0.05$.

supplemented with 5% FBS, 1% penicillin/streptomycin at 37 °C and 5% CO_2. For the treatments, 2.5×10^5 cells/well in 3 mL medium were plated in 6-well tissue culture dishes for twenty-four hours. Then, the medium was replaced with fresh one (control group), or supplemented with 30 μL of EVs derived from either control or CF-MSCs (ctr EVs and CF-EVs group, respectively) for 24 h. Cells were then harvested to perform different assays. Cell viability was evaluated by Trypan blue exclusion test as previously reported (Fabiani et al., 2017).

2.6. EV uptake

Five millions ctr MSCs and CF-MSCs were labeled with CellBrite Green Cytoplasmic Membrane Dye (Biotium) according to the manufacturer's instructions and supernatants were collected after 72 h and used to isolate EVs' populations by ultracentrifugation. IB3-1 cells were seeded in 24-well culture plates and treated for 16 h with 100 μL of either ctr- or CF-EVs suspension obtained by resuspension in 500 μL of IB3-1 cell medium. Then, the cells were trypsinized and analyzed by flow cytometry.

2.7. Nanoparticle tracking analysis (NTA) of EVs

The size and total number of EVs were calculated with the technology of Nanoparticle Tracking Analysis (NTA) that allows measuring the Brownian motion of suspended vesicles (Pergoli et al., 2017). By using the NanoSight NS300 system (Amesbury, UK), five 30-s recordings were made for each sample and the data were analyzed with NTA software. In order to eliminate the presence of vesicles derived from FBS in the medium, EVs samples were obtained from ctr- and CF-MSCs cultured in FBS free medium for 24 h. The results are provided as high-resolution particle-size distribution and particles concentration.

2.8. Laser light scattering analysis of EVs

Parallel Dynamic and Static Laser Light Scattering (DLS and SLS) experiments were performed on a home-made apparatus equipped with four optical channels, to reach high sensitivity (Lago and Rovati, 1993). Samples were inserted in a quartz cell kept at 25 °C or 37 °C. Light scattering measurements gave information on molecular mass of the particles in solution and on their translational diffusion coefficient, related to their hydrodynamic radius. DLS data were analyzed by both the cumulants method, to detect the weight-average hydrodynamic size of particles, and the non-negative least-squares (NNLS) method (Lawson and Hanson, 1995), suitable to determine the size distribution of EVs. EVs samples were prepared as described for NTA analysis and observed by light scattering to verify the presence/absence of particles in the same size range of EVs. All samples were diluted 1:10 with filtered PBS to avoid multiple scattering.

2.9. Sphingolipid profile of EVs and MSCs

Sphingolipid extraction and LC–MS/MS evaluation were performed according to the procedure already published elsewhere (Platania et al., 2019). Briefly, in order to increase the recovery of low-abundance sphingolipids, samples were extracted by a monophasic Bligh-Dyer method with alkaline methanolysis. Purified samples (10 μL) were directly injected to LC–MS/MS instrumentation (UPLC Dionex 3000 UltiMate - Thermo Fisher Scientific, USA) connected to an ABSciex 3200 QTRAP - AB Sciex S.r.l., Milano, Italy) for quantitative analysis. Separation was attained on a reversed-phase BEH C-8 10 × 2.1 x 1.7 μm analytical column with a linear gradient obtained by mixing eluent A (water + 2 mM ammonium formate + 0.2% formic acid) and eluent B (methanol + μ ammonium formate + 0.2% formic acid). Multiple reaction monitoring (MRM) mode was used. For ceramides and dihydroceramides quantitative analysis was performed interpolating each peak area of analyte/area IS (200 pmol Cer C12) with a calibration curve of each sphingolipid. For sphingomyelins, since the standards were not available, relative quantification was achieved by the ratio of the analyte/area IS (200 pmol SM C12). Then, sphingolipids amount was normalized by total protein content, expressed in milligram, in each sample.

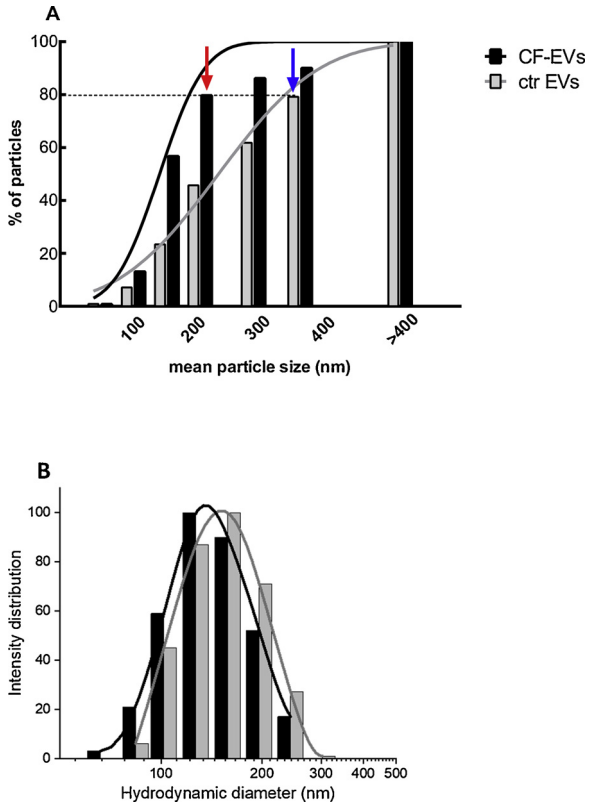

Fig. 2. Morphological features of ctr and CF-EVs populations. Panel **A** shows an example of Nanoparticle Tracking Analysis (NTA) representing the overall distribution of the particles in ctr and CF-EV populations, according to their mean size. On the cumulative plot, data are reported as percentage of particles distributed within a mean size value, expressed as nm. Panel **B** reports an example of Dynamic Light Scattering analysis showing the intensity weighted distribution of hydrodynamic diameters for ctr EVs and CF-EVs. The black bars and the corresponding black plotting curve refer to CF-EV. The gray bars and the corresponding plotting curve refer to EVs from control MSCs. The graphs are the most representative of four different analysis.

2.10. RNA extraction and quantitative RT-PCR

Real-time PCR was performed on RNA from control and ctr EVs and CF-EVs-treated IB3-1 ($2{,}5 \times 10^5$ cells/well). RNA extraction and reverse transcription were performed as previously reported (Zulueta et al., 2018). Human gene primer sequences for SPTLC 1, SPTLC 2, SPTLC 3, nSMase2, PPARγ, IL-1β, IL-8, IL-6 and GAPDH were previously published (Zulueta et al., 2018; Hornemann et al., 2006; Kubota et al., 2015; Dechecchi et al., 2011). RT-PCRs were performed on a StepOnePlus Real-Time PCR Systems (Thermofisher). Results were normalized on GAPDH and the 2-ΔΔCt method was used to calculate the relative value of gene expression *vs* control cells (Arocho et al., 2006). Determinations were done in triplicate.

2.11. Protein extraction and western blotting

Nuclear and cytoplasmic extracts from 5×10^5 IB3-1 cells, either treated or not with EVs, were obtained with the NE-PER Nuclear and Cytoplasmic Extraction Reagents kit (Thermo scientific) according to the manufacturer's instructions, for PPARγ evaluation. To characterize CFTR channel expression, whole cell lysates were prepared by trypsinization of treated and control MSCs, washed in cold PBS containing protease inhibitors, centrifuged at 800 g for 5 min at 4 °C, and finally resuspended in the same PBS solution. Equal amounts of nuclear (10 μg) or cytoplasmic (20 μg) protein's extracts were resuspended in Laemmli solution, separated by electrophoresis and immunoblotted as previously described (Fabiani et al., 2017). Anti-PPARγ (1:500 in TBS-T), anti HO-1 (1:1000 in TBS-T), anti-caspase 9 (1:1000 in TBS-T), anti-LC3 (1:1000 in TBS-T), anti-β-Actin (1:5000 in TBS-T), and anti-H3 (1:500 in TBS-T) antibodies were used. H3 and β-Actin contents were quantified for data normalization of nuclear and cytoplasmic markers, respectively. Specific bands intensity, as revealed by chemiluminescence, was quantified by Alliance UVITEC Cambridge.

2.12. ELISA determinations

The protein expression of the cytokines IL-1β, IL-6 and IL-8 was determined in treated IB3-1 culture media by biomarker multiplex immunoassays on Luminex® Platform. Cell protein concentration, was calculated by Bradford assay and used for data normalization. Determinations have been performed in duplicate.

2.13. Ferric reducing antioxidant power (FRAP) assay

The ferric reducing antioxidant power (FRAP) assay was performed according to previously published method (Benzie and Strain, 1999) with minor modifications (Zulueta et al., 2017).

2.14. Statistical analysis

Data significance was evaluated by paired two-tailed Student *t*-test and by one-way ANOVA followed by the Newman-Keul post-test when significant ($P < 0.05$). The results are the mean value (mean ± SEM) from five to seven individual experiments, depending on the assay. Either duplicate or triplicate samples for each treatment were performed. Western blotting, light scattering and flow cytometry images are the most representative. Statistical analysis was performed by GraphPad Instat software (La Jolla, CA, USA) and graph illustrations by GraphPad Prism software (La Jolla, CA, USA).

3. Results

3.1. EVs released from ctr- and CF-MSCs differently attenuate the pro-inflammatory profile of IB3-1 cells

In order to investigate the hypothesis that lung MSCs and MSC-derived EVs could be immunologically impaired in CF, we obtained an *in vitro* model of CF-MSCs, by treating control MSCs with the specific CFTR inhibitor, I-172 (Mattoscio et al., 2010). At first, we confirmed by Western Blotting analysis that lung MSCs express CFTR protein as it is shown in Supplementary Fig. 1. IB3-1 cells cultured in basal condition, were treated for 24 h with 30 μL of EVs released from either I-172-treated or untreated MSCs (namely CF-EVs or ctr EVs). The cell viability was unaffected by the treatment with CF-EVs and neither signs of early apoptosis nor of autophagy were increased as compared to the ctr EVs-treated cells (Supplementary Fig. 2). Concerning the expression of pro-inflammatory cytokines, following ctr EVs supplementation we observed a trend toward a decrease in the mRNA and protein expression of IL-1β, IL-8 and IL-6 vs control IB3-1 cells not supplemented (Fig. 1). IL-1β seems the most responsive, showing a significant 35% reduction at both the transcriptional and the protein level (Fig. 1, panel A;B) though IL-6 protein amount moves from 95.4 ± 11.4 to 56.6 ± 2.5 pg/mg protein, with a global 40% reduction (Fig. 1, panel F).

As a whole, CF-EVs seem less effective then ctr EVs in attenuating the pro-inflammatory profile of IB3-1 cells. Both the mRNAs and the proteins of the three cytokines slightly increased in the CF-EVs group as compared to the ctr EVs group, though not significantly exceeding the control basal level (Fig. 1). Notably, we observed significant differences in IL-1 β mRNA (Fig. 1, panel A) and IL-6 protein (Fig. 1, panel F) which are significantly higher in the CF-EVs treated group than in the ctr EVs one. In fact, IL-1β mRNA rises by about 45% and IL-6 protein by 60%, moving from 56.6 ± 2.5 to 90.49 ± 8.28 pg/mg protein.

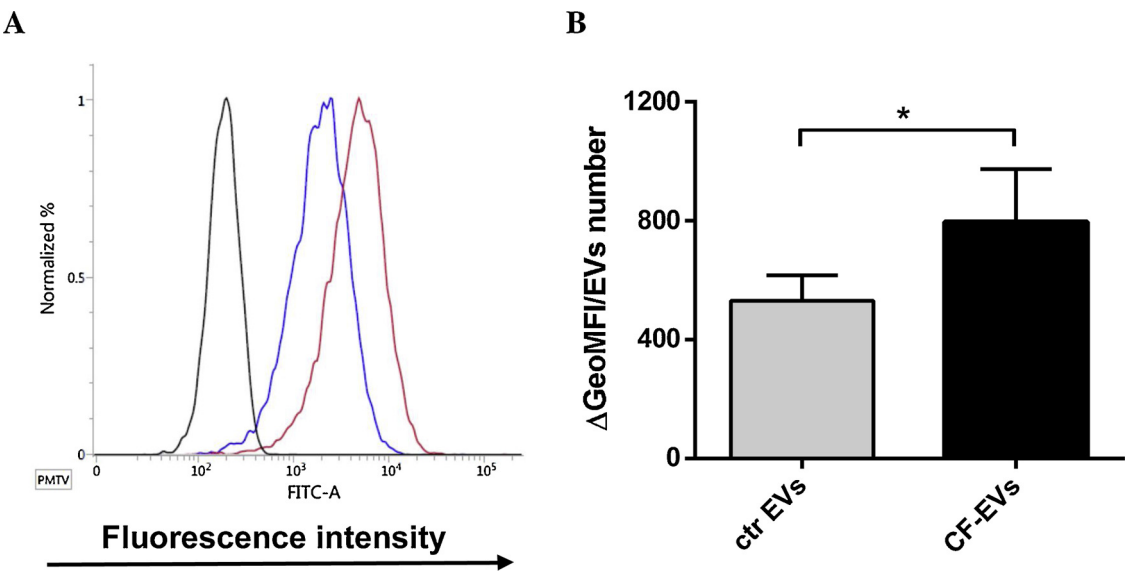

Fig. 3. Labeled EVs incorporation by IB3-1 cells. IB3-1 cells were seeded in 24-well culture plates and treated for 16 h with 100 µL of EVs derived from CellBrite Green Cytoplasmic Membrane Dye-labeled MSCs. Panel **A**: representative graph of the fluorescence intensity values indicating the uptake rate of EVs. The black curve represents the untreated cells; the blue curve represents cells incubated with ctr EVs and the red curve represents cells incubated with CF-EVs. Panel **B**: quantitative determination of EVs uptake by IB3- 1 cells following 16 h of incubation. The gray and black bars represent the internalization value of EVs released from control and CF-MSCs, meaning MSCs added with 10 µg/ml of CFTR inhibitor, I-172, for 48 h. Data are expressed as mean ± SEM of five independent experiments. The statistical significance was evaluated by two-tailed, paired, Student *t*-test (*, $P < 0.05$) performed on the value of geometric mean fluorescent intensity subtracted of the control untreated cells (ΔGeoMFI) and normalized on the number of particles (For interpretation of the references to colour in this figure legend, the reader is referred to the web version of this article.).

We have recently demonstrated that PPARγ, which has an established anti-inflammatory role, is up-regulated in the IB3-1 cell line upon treatment with ctr MSCs-derived EVs (Zulueta et al., 2018). Conversely, here we show that PPARγ transcript is unaffected by CF-EVs treatment, being expressed as in the untreated control IB3-1 cells (Supplementary Fig. 3), supporting the hypothesis of CF-EVs immunological impairment. The EV treatment could interfere with the redox homeostasis of IB3-1 cells, thus indirectly modulating the inflammation status (Supplementary Fig. 4). Control-EVs increase the intrinsic antioxidant power of IB3-1 cells, as shown by the rise in the Fe ions level in the reduced form and by the up-regulation of HO-1 that is a master regulator of the redox-homeostasis. Conversely, CF-EVs treatment fails in improving this protective response, as evidenced by the content of Fe ions in the reduced form and HO-1 that are pretty near to the control value.

3.2. EVs from ctr- and CF-MSCs show different features

We have already specified the composition of the EV population released by human lung MSCs by the classical exosome and microvesicle markers (Zulueta et al., 2018). In this project, we aimed at characterizing ctr EV and CF-EVs in order to understand whether they possess distinct features that might partially account for their different anti-inflammatory potential.

We evaluated the amount of EVs and their size distribution by both Nanoparticles Tracking Analysis (NTA) and Light Scattering. Fig. 2 reports structural result of ctr EVs and CF-EVs prepared in serum-free medium, as described in "material and methods" section, to better characterize the differences among the two particle populations. The cumulative frequency plot (Fig. 2, panel A) shows that ctr EVs exhibit a wide regular distribution with approximately 80% particles distributed within 340 nm in size (as indicated by the blue arrow). Conversely, CF-EVs rather follow a Gaussian distribution that peaks at 150 nm, with approximately 80% particles within 200 nm (as indicated by the red arrow). Those results are in agreement with the mean hydrodynamic size, as assessed by Dynamic Light Scattering (Fig. 2, panel B). As shown, CF-EVs have a hydrodynamic size 20% smaller than the ctr EVs, corresponding to about a 60% smaller volume per EV. Moreover, both NTA and light scattering experiments determined that the number of CF-EVs was approximately 1.5 times higher than the number of ctr EVs, moving from $4.27 \times 10^9 \pm 5.5 \times 10^8$ to $2.99 \times 10^9 \pm 8.0 \times 10^8$/ml (NTA data, not shown). The combined results suggest that EVs released by ctr MSCs and CF-MSCs, have a different supramolecular organization, resulting in more numerous, but smaller CF-EVs.

To study the internalization rate of MSCs-derived EVs by IB3-1 cells, we designed a quantitative flow cytometric assay, as reported in the "Materials and methods" section. Control and CF-MSCs were labeled with the CellBrite Cytoplasmic Membrane Dye, EVs were isolated and used to treat IB3-1 cells and the uptake was assessed by flow cytometry 16 h later. Fig. 3 shows that CF-EVs are more efficiently internalized by IB3-1 cells than ctr EVs, as indicated by the value of the fluorescence intensity, normalized on the number of particles, with an increase of almost 50% (from 531.3 ± 84.63–795.8 ± 177.3 ΔGeoMFI/EVs number).

3.3. Sphingolipid profile is differently characterized in ctr EVs and CF-EVs

In an attempt to gain insights in the potential mediators underlying the different anti-inflammatory behavior of ctr- and CF-EVs, we determined the composition of SPLs that play a well-known role in modulating inflammation. By means of LC–MS/MS analysis, we observed a significant rise in the content of total Cer and dhCer, its precursor along the neo synthesis pathway, in CF-EVs *vs* ctr EVs, with value ranging from 790.9 ± 76.3 to 991.1 ± 133.8 and from 18.17 ± 1.8 to 25.75 ± 3.7 pmoles/mg protein, respectively (Table 1).

When considering the single Cer species (Fig. 4, panel D), we found that the most representative fatty acid containing Cer is the C16:0 which accumulates in CF-EVs 15% more than in ctr EVs. Moreover, the ceramides bearing longer saturated and unsaturated fatty acid chains, namely C20:0, C22:0, C24:0, and C24:1, significantly increased in CF-EVs by 25%, 60%, 100%, and 25%, respectively. We observed the same trend in the corresponding dhCer species. As shown in panel E, dhC16-

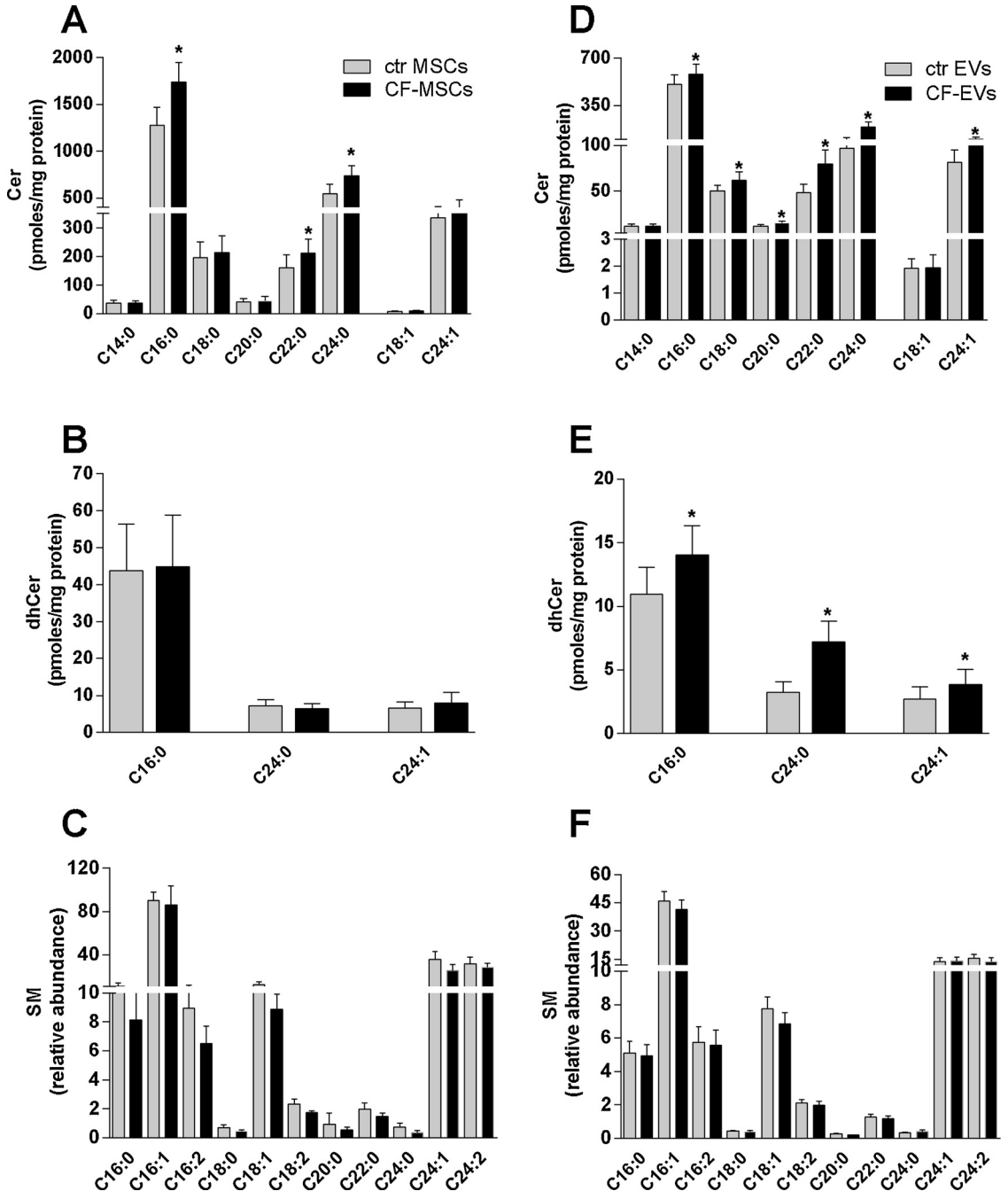

Fig. 4. Sphingolipid profile of ctr and CF-EVs and parental MSCs. Sphingolipid profile of EVs and parental MSCs was obtained by LC/MS analysis. Panel **A** and **D** represent single Cer species content, expressed as pmoles/mg protein, in MSCs and EVs populations, respectively. Panel **B** and **E** show single dhCer species content, reported as pmoles/mg protein, in MSCs and EVs populations, respectively. Panel **C** and **F** represent single SM species content, expressed as relative abundance, in MSCs and EVs populations, respectively. The gray bars correspond to ctr MSCs and ctr EVs while the black bars refer to CF-MSCs and CF-EVs. Data are expressed as mean ± SEM of five to seven independent experiments. The statistical significance was evaluated by two-tailed, paired, Student *t*-test (*, $P < 0.05$).

Cer rises by almost 30%, dhC24:0-Cer by more than twofold and dhC24:1-Cer by 40%. As for SM, we found no significant differences in the total (Table 1) and the single species expression (Fig. 4, panel F) but only a trend toward a decrease in their level was apparent. As compared to EVs, parental MSCs cells display a similar SPLs pattern. We observed a significant 30% increase in the total Cer content (from 2605 ± 461.4–3387 ± 496.8 pmoles/mg protein; Table 1) and about 35% accumulation of the most representative fatty acid containing Cer, namely C16:0, C22:0, and C24:0 (Fig. 4, panel A). On the contrary, total (Table 1) and single dhCer species (Fig. 4, panel B) were similarly expressed in both MSC populations. Finally, we found a reduction in the relative abundance of total and single SM species (Table 1; Fig. 4, panel C).

Next, we checked whether the ctr and the CF-MSCs, could differently express the Serine palmitoyl transferase (SPT), the rate limiting enzyme of the *de novo* ceramide biosynthesis pathway, and the neutral sphingomyelinase 2 (n-SMase 2), highly involved in the biogenesis of EVs. SPTLC-2 mRNA (panel A), one of the two catalytic subunits of SPT, as well as n-SMase 2 (panel B) were significantly upregulated (*, $p = 0.04$ and *, $p = 0.02$, respectively) in CF-MSCs as compared to ctr MSCs (Fig. 5).

Table 1
Total sphingolipid content in ctr and CF-EVs and parental MSCs. Total Cer and dhCer content was assessed by LC–MS/MS. The results are expressed as pmoles/mg protein. For total SM content, relative quantification was achieved by the ratio of the analyte/area IS (200 pmol SM C12). Data, reported as mean ± SEM, are obtained from five to seven independent experiments. The statistical significance was evaluated by two-tailed, paired, Student *t*-test.

Total	Cer pmoles/mg protein	dhCer pmoles/mg protein	SM relative abundance
Ctr MSCs	2605 ± 461.4 (n = 5)	55.68 ± 13.1 (n = 5)	195.1 ± 30.7 (n = 5)
CF-MSCs	3387 ± 496.8 (n = 5) P = 0.02	57.36 ± 15.9 (n = 5) P = ns	168 ± 30.2 (n = 5) P = 0.03
Ctr EVs	790.9 ± 76.3 (n = 7)	18.17 ± 1.8 (n = 7)	98.24 ± 11.7 (n = 7)
CF-EVs	991.1 ± 133.8 (n = 7) P = 0.04	25.75 ± 3.7 (n = 7) P = 0.01	90.87 ± 11.5 (n = 7) P = ns

4. Discussion

Our study focuses on determining whether MSCs could impact the inflammatory chronic condition that characterizes Cystic Fibrosis. We took advantage of an *in vitro* cellular model of CF-MSC by treating control human lung MSCs with a specific CFTR inhibitor (I-172) in order to obtain CF-EVs that mimic those particles physiologically released in the lung of CF patient. We used IB3-1, a transformed human bronchial epithelial cell line from a CF patient (ΔF508/W1282X), to gain the basal inflammatory CF phenotype (Armstrong et al., 1997; Tirouvanziam et al., 2000) and we compared the anti-inflammatory potential of CF-EVs with control EVs. As we previously published (Zulueta et al., 2018), here we show that EVs from control MSCs attenuate the pro-inflammatory profile of IB3-1 cell by reducing the cytokines expression and rescuing the transcription of PPARγ, highly involved in anti-inflammatory mechanisms. On the contrary, CF-EVs treatment is less effective on cytokines and PPARγ expression, providing an explanation for the basal physiological inflammatory phenotype. Accordingly, Sutton and colleagues (Sutton et al., 2017) recently showed that deficient CFTR function, achieved by the same CFTR inhibitor (I-172), alters human MSCs ability to control the inflammatory response to pathogenic organisms. They indicate that CF-MSCs do not behave similarly to control MSCs, due to the expression of different amounts of IL-6, CCL2 and IL-8. Moreover, they observed that by blocking CFTR activity in wild type bone marrow derived macrophages, PPARγ levels decrease.

Our results suggest that the two EVs populations released by the parental MSCs, exhibit quite different features. CF-EVs are more abundant and smaller than the ctr EVs and they are more efficiently uptaken by the recipient IB3-1 cells. Growing evidence indicates that inflammatory conditions might trigger the release of EVs that in turn maintain such condition. As reviewed by Cypryk and colleagues (Cypryk et al., 2018), inflammasome activity correlates with enhanced secretion of EVs and modulation of their mediators content. Murine microglial cell line challenged with LPS, acquires an activated pro-inflammatory status that greatly increases the release of EVs. In contrast, EV secretion was completely attenuated to control levels using a TNFα inhibitor (Yang et al., 2018). In our experimental model, we did not directly challenge MSCs with pro-inflammatory stimuli, but CF-MSCs seem to be immunological impaired since CFTR activity inhibition is *per se* correlated to inflammation (Sutton et al., 2017), thus enhancing EVs secretion. Though the ESCRT machinery represents the general process of exosomes release, in 2008 a Cer-mediated mechanism has been first described (Trajkovic et al., 2008). The authors proposed SM hydrolysis by n-SMase 2, the enzyme which mostly resides in the Golgi and ER, and the consequent Cer generation as important players in exosomes biogenesis. In fact, the cone-shaped structure of Cer spontaneously drives the negative curvature of the membrane, favouring vesicles formation. Consistently, the block of n-SMase reduces exosomes release in various cell lines (Kosaka et al., 2010; Asai et al., 2015; Xu et al., 2016). However, the same enzyme differentially controls the secretion of larger EV population, such as MVs (Menck et al., 2017). We found a significant decrease in the relative abundance of total SM in CF-MSCs *versus* ctr MSCs, together with a transcriptional activation of n-SMase 2, suggesting that this pathway could be involved in EVs production.

Therefore, the accumulation of Cer observed in both CF-EVs and parental MSCs, could contribute to the abundancy of CF-EVs as compared to ctr EVs. Ceramide formation upon SM hydrolysis, allows those membrane changes required for the release of exosomes that are on average smaller than MVs, thus accounting for the majority of CF-EVs distributed within 150 nm in size, as compared to ctr EVs. In our model, the significant accumulation of both Cer and dhCer species in CF-EVs points to the involvement of the *de novo* Cer synthesis in the parental CF-MSCs. This finding is further supported by the transcriptional up-regulation of SPLTC-2, one of the two catalytic subunits of the SPT that regulates the rate limiting step of the *de novo* pathway. Though CF-MSCs exhibit unchanged dhCer levels, specific mechanisms of lipid sorting into EVs that export out of the cells the SPLs generated could occur (Podbielska et al., 2016). The higher content in dihydroceramides of EVs in comparison to MSCs, suggests that the Cer biosynthesis up-regulation is tightly linked to the extrusion of signaling lipids, deriving from ER and including Cer precursor. Whereas this latter is rapidly

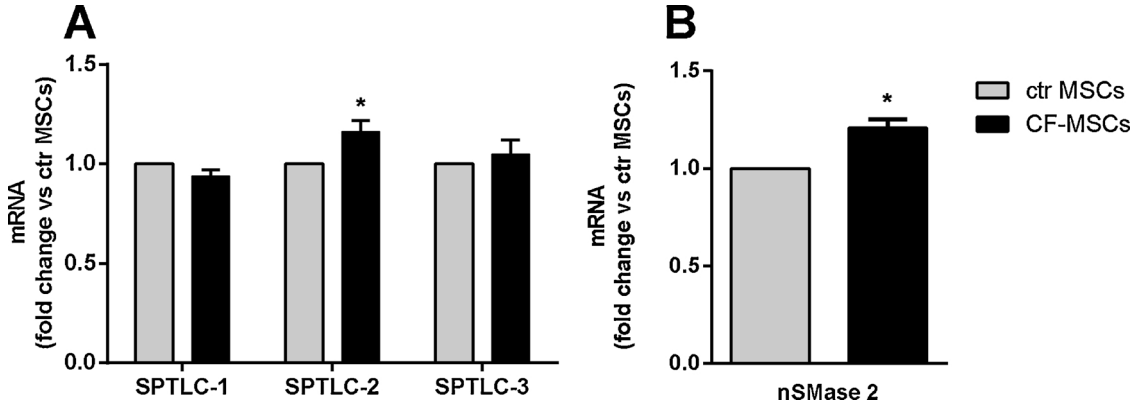

Fig. 5. mRNA expression of Serine palmitoyl transferase (SPT) and neutral sphingomyelinase 2 (n-SMase 2) in ctr and CF-MSCs. Control MSCs (ctr MSCs, gray bar) refer to untreated MSCs while CF-MSCs (black bar), refer to control MSCs treated for 48 h with 10 μg/ml of CFTR inhibitor, I-172. The results are expressed as fold change over the control MSCs. Data, reported as mean ± SEM, are obtained from five independent experiments. For each treatment, the samples were run in triplicate. The statistical significance was evaluated by two-tailed, paired, Student *t*-test.

dehydrogenated along with ER reactions, its early compartmentalization in multi-vesicular bodies may fuel extracellular lipid signaling in the effort of controlling lipid cellular homeostasis. Our results indicate that the inflammation activated Cer *de novo* synthesis and accumulation (Caretti et al., 2014; Caretti et al., 2016) trigger a transcriptionally driven response that requires higher sphingomyelinase activity to sustain the release of new formed ceramide throughout the exocytosis of vesicles that spread their originating inflammatory-alarm signal.

It has been reported that Cer-enriched exosomes mediate cytotoxic effects in recipient cells. Podbielska and colleagues (Podbielska et al., 2016) demonstrated that HOG, an oligodendroglioma cell line, responds to cytotoxic cytokines by eliciting the release of Cer-enriched exosomes. They support the idea that vesicular Cer contributes *per se* to the toxic effects elicited by the cytokines. This is consistent with previous studies illustrating that many dangerous effects of TNFα on different subsets of cells are mediated by Cer generation (Osawa et al., 2005; White-Gilbertson et al., 2009). Similarly, we have previously published that Cer from *de novo* biosynthesis pathway contributes to lung inflammation in CF murine models, upon infection with *P. aeruginosa* and *A. fumigatus* (Caretti et al., 2014; Caretti et al., 2016). Our present results corroborate these data since we found an inverse correlation between the anti-inflammatory efficacy of EVs and their Cer content.

5. Conclusion

In conclusion, our findings support the hypothesis that CFTR dysfunction, obtained by treating control MSCs with a specific CFTR inhibitor, associates with an enhanced sphingolipid metabolism leading to an increase in the content of ceramide. This in turn promotes the release of CF-EVs that export the excess of pro-inflammatory ceramide to the recipient cells, thus contributing to maintain the chronic, unresolved inflammatory status of Cystic Fibrosis. These results contribute to better elucidate the role of Cer-enriched EVs in Cystic Fibrosis, providing the rationale for novel therapeutic approaches.

Declaration of Competing Interest

The authors declare no conflict of interest.

Acknowledgments

A. Zulueta post doc position was funded by the University of Milan, Italy. V. Peli was granted by the University of Milan, Italy, “Borse Giovani promettenti laureati”. M. Dei Cas was supported by the PhD program in “Molecular and Translational Medicine” of the University of Milan, Italy. M. Colombo was granted by Fondazione Italiana per la Ricerca sul Cancro (post-doctoral fellowship 18013). EDF thanks BIOMETRA Dept. for in house support. AC thanks Dr. Andrea Brizzolari for FRAP assay. This work was supported by the University of Milan, Italy, Piano di Sostegno alla Ricerca 2015/2017, finanziamento LINEA 2″Dotazione annuale per attività istituzionale"

Appendix A. Supplementary data

Supplementary material related to this article can be found, in the online version, at doi:https://doi.org/10.1016/j.biocel.2019.105622.

References

Armstrong, D.S., et al., 1997. Lower airway inflammation in infants and young children with cystic fibrosis. Am. J. Respir. Crit. Care Med. 156 (4 Pt 1), 1197–1204.
Arocho, A., et al., 2006. Validation of the 2-DeltaDeltaCt calculation as an alternate method of data analysis for quantitative PCR of BCR-ABL P210 transcripts. Diagn. Mol. Pathol. 15 (1), 56–61.
Asai, H., et al., 2015. Depletion of microglia and inhibition of exosome synthesis halt tau propagation. Nat. Neurosci. 18 (11), 1584–1593.
Becker, K.A., et al., 2010. Accumulation of ceramide in the trachea and intestine of cystic fibrosis mice causes inflammation and cell death. Biochem. Biophys. Res. Commun. 403 (3–4), 368–374.
Benzie, I.F., Strain, J.J., 1999. Ferric reducing/antioxidant power assay: direct measure of total antioxidant activity of biological fluids and modified version for simultaneous measurement of total antioxidant power and ascorbic acid concentration. Methods Enzymol. 299, 15–27.
Bianco, F., et al., 2009. Acid sphingomyelinase activity triggers microparticle release from glial cells. EMBO J. 28 (8), 1043–1054.
Bonzini, M., et al., 2017. Short-term particulate matter exposure induces extracellular vesicle release in overweight subjects. Environ. Res. 155, 228–234.
Caretti, A., et al., 2014. Anti-inflammatory action of lipid nanocarrier-delivered myriocin: therapeutic potential in cystic fibrosis. Biochim. Biophys. Acta 1840 (1), 586–594.
Caretti, A., et al., 2016. Inhibition of ceramide de novo synthesis by myriocin produces the double effect of reducing pathological inflammation and exerting antifungal activity against A. fumigatus airways infection. Biochim. Biophys. Acta 1860 (6), 1089–1097.
Chiricozzi, E., et al., 2018. Sphingolipids role in the regulation of inflammatory response: from leukocyte biology to bacterial infection. J. Leukoc. Biol. 103 (3), 445–456.
Cypryk, W., Nyman, T.A., Matikainen, S., 2018. From inflammasome to exosome-does extracellular vesicle secretion constitute an inflammasome-dependent immune response? Front. Immunol. 9, 2188.
Dechecchi, M.C., et al., 2011. Modulators of sphingolipid metabolism reduce lung inflammation. Am. J. Respir. Cell Mol. Biol. 45 (4), 825–833.
Dinkins, M.B., et al., 2014. Exosome reduction in vivo is associated with lower amyloid plaque load in the 5XFAD mouse model of Alzheimer’s disease. Neurobiol. Aging 35 (8), 1792–1800.
Dostert, G., et al., 2017. How do mesenchymal stem cells influence or are influenced by microenvironment through extracellular vesicles communication? Front. Cell Dev. Biol. 5, 6.
Fabiani, C., et al., 2017. 2-Acetyl-5-tetrahydroxybutyl imidazole (THI) protects 661W cells against oxidative stress. Naunyn Schmiedebergs Arch. Pharmacol. 390 (7), 741–751.
Fatima, F., et al., 2017. Non-coding RNAs in mesenchymal stem cell-derived extracellular vesicles: deciphering regulatory roles in stem cell potency, inflammatory resolve, and tissue regeneration. Front. Genet. 8, 161.
Gault, C.R., Obeid, L.M., Hannun, Y.A., 2010. An overview of sphingolipid metabolism: from synthesis to breakdown. Adv. Exp. Med. Biol. 688, 1–23.
Grassme, H., Riethmuller, J., Gulbins, E., 2013. Ceramide in cystic fibrosis. Handb. Exp. Pharmacol. (216), 265–274.
Hannun, Y.A., Obeid, L.M., 2008. Principles of bioactive lipid signalling: lessons from sphingolipids. Nat. Rev. Mol. Cell Biol. 9 (2), 139–150.
Hornemann, T., et al., 2006. Cloning and initial characterization of a new subunit for mammalian serine-palmitoyltransferase. J. Biol. Chem. 281 (49), 37275–37281.
Kosaka, N., et al., 2010. Secretory mechanisms and intercellular transfer of microRNAs in living cells. J. Biol. Chem. 285 (23), 17442–17452.
Kubota, S., et al., 2015. Secretion of small/microRNAs including miR-638 into extracellular spaces by sphingomyelin phosphodiesterase 3. Oncol. Rep. 33 (1), 67–73.
Lago, P., Rovati, L., 1993. A quasielastic light scattering detector for chromatographic analysis. Rev. Sci. Instrum. 64 (7), 1797–1802.
Lawson, C.L., Hanson, R.J., 1995. Solving Least Squares Problems. SIAM, Philadelphia.
Marchesini, N., Hannun, Y.A., 2004. Acid and neutral sphingomyelinases: roles and mechanisms of regulation. Biochem. Cell Biol. 82 (1), 27–44.
Mattoscio, D., et al., 2010. Cystic fibrosis transmembrane conductance regulator (CFTR) expression in human platelets: impact on mediators and mechanisms of the inflammatory response. FASEB J. 24 (10), 3970–3980.
Menck, K., et al., 2017. Neutral sphingomyelinases control extracellular vesicles budding from the plasma membrane. J. Extracell. Vesicles 6 (1) p. 1378056.
Osawa, Y., et al., 2005. Roles for C16-ceramide and sphingosine 1-phosphate in regulating hepatocyte apoptosis in response to tumor necrosis factor-alpha. J. Biol. Chem. 280 (30), 27879–27887.
Pergoli, L., et al., 2017. Extracellular vesicle-packaged miRNA release after short-term exposure to particulate matter is associated with increased coagulation. Part. Fibre Toxicol. 14 (1), 32.
Petrache, I., Petrusca, D.N., 2013. The involvement of sphingolipids in chronic obstructive pulmonary diseases. Handb. Exp. Pharmacol. (216), 247–264.
Platania, C.B.M., et al., 2019. Novel ophthalmic formulation of myriocin: implications in retinitis pigmentosa. Drug Deliv. 26 (1), 237–243.
Podbielska, M., et al., 2016. Cytokine-induced release of ceramide-enriched exosomes as a mediator of cell death signaling in an oligodendroglioma cell line. J. Lipid Res. 57 (11), 2028–2039.
Riethmuller, J., et al., 2009. Therapeutic efficacy and safety of amitriptyline in patients with cystic fibrosis. Cell. Physiol. Biochem. 24 (1–2), 65–72.
Subra, C., et al., 2007. Exosome lipidomics unravels lipid sorting at the level of multivesicular bodies. Biochimie 89 (2), 205–212.
Sutton, M.T., et al., 2017. Mesenchymal stem cell soluble mediators and cystic fibrosis. J. Stem Cell Res. Ther. 7 (9).
Teichgraber, V., et al., 2008. Ceramide accumulation mediates inflammation, cell death and infection susceptibility in cystic fibrosis. Nat. Med. 14 (4), 382–391.
Tirouvanziam, R., et al., 2000. Inflammation and infection in naive human cystic fibrosis airway grafts. Am. J. Respir. Cell Mol. Biol. 23 (2), 121–127.
Trajkovic, K., et al., 2008. Ceramide triggers budding of exosome vesicles into multivesicular endosomes. Science 319 (5867), 1244–1247.
Verderio, C., Gabrielli, M., Giussani, P., 2018. Role of sphingolipids in the biogenesis and biological activity of extracellular vesicles. J. Lipid Res. 59 (8), 1325–1340.
Wang, G., et al., 2012. Astrocytes secrete exosomes enriched with proapoptotic ceramide

and prostate apoptosis response 4 (PAR-4): potential mechanism of apoptosis induction in Alzheimer disease (AD). J. Biol. Chem. 287 (25), 21384–21395.
White-Gilbertson, S., et al., 2009. Ceramide synthase 6 modulates TRAIL sensitivity and nuclear translocation of active caspase-3 in colon cancer cells. Oncogene 28 (8), 1132–1141.
Xu, Y., et al., 2016. Macrophages transfer antigens to dendritic cells by releasing exosomes containing dead-cell-associated antigens partially through a ceramide-dependent pathway to enhance CD4(+) T-cell responses. Immunology 149 (2), 157–171.
Yang, Y., et al., 2018. Inflammation leads to distinct populations of extracellular vesicles from microglia. J. Neuroinflammation 15 (1), 168.
Yuyama, K., et al., 2012. Sphingolipid-modulated exosome secretion promotes clearance of amyloid-beta by microglia. J. Biol. Chem. 287 (14), 10977–10989.
Zulueta, A., et al., 2018. Lung mesenchymal stem cells-derived extracellular vesicles attenuate the inflammatory profile of Cystic Fibrosis epithelial cells. Cell. Signal. 51, 110–118.
Zulueta, A., et al., 2017. Inhibitors of ceramide de novo biosynthesis rescue damages induced by cigarette smoke in airways epithelia. Naunyn Schmiedebergs Arch. Pharmacol. 390 (7), 753–759.